Journal of Power Sources 403 (2018) 109–117

Contents lists available at ScienceDirect

Journal of Power Sources

journal homepage: www.elsevier.com/locate/jpowsour

All-printed solid-state substrate-versatile and high-performance micro-supercapacitors for *in situ* fabricated transferable and wearable energy storage via multi-material 3D printing

Yan Zhang[a], Tengxiao Ji[a], Shihui Hou[b], Lifang Zhang[a], Yunhui Shi[a], Jingxin Zhao[a], Xinhua Xu[a,c,*]

[a] School of Materials Science and Engineering, Tianjin University, Tianjin, 300072, PR China
[b] School of Chemical Engineering and Technology, Tianjin University, Tianjin, 300072, PR China
[c] Tianjin Key Laboratory of Composite and Functional Materials, Tianjin University, Tianjin, 300072, PR China

HIGHLIGHTS

- Printed micro-supercapacitors were fabricated on different substrates.
- Successful synthesis of new-type polypyrrole/polyaniline coaxis nanotubes.
- A complex 3D printed energy storage device with 484 retractions was built.
- Tape-type micro-supercapacitors were developed for easy transferable electronics.
- An *in situ* fabricated micro-supercapacitor on lab-gown for wearable applications.

GRAPHICAL ABSTRACT

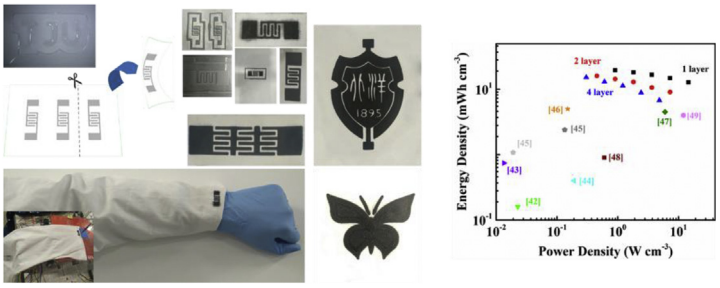

ARTICLE INFO

Keywords:
Micro-supercapacitors
3D printing
Substrate-versatile
In situ fabricated
Wearable electronics

ABSTRACT

Micro-supercapacitors are a kind of state-of-the-art energy storage devices and have great potential to be developed in portable and wearable electronics. Here, we report a novel strategy for scalable fabrication of all-printed solid-state micro-supercapacitors with multilayer structure via multi-material 3D printing technique. To obtain electrode materials, we synthesize polypyrrole/polyaniline coaxis nanotubes by utilizing the self-degraded template polymerization method and *in situ* electrochemical polymerization. The as-prepared aqueous composite electrode ink shows significant shear thinning behavior and excellent processability: a complex electrode patterning with 484 retractions was proved. In addition, the inks are well-adapted to various substrates (paper, texitle, plastic film etc), allowing the device to be printed onto different substrates, even directly on the desired surface. As a conceptual exhibition, we design two schemes of *in situ* fabricated energy storage devices to meet the ever-changing energy needs and expand the application range of micro-supercapacitors. The transferable tape-type micro-supercapacitors can be stuck to any surfaces where energy is needed immediately. The *in situ* fabricated wearable micro-supercapacitor on lab-gown shows promising performance and excellent flexibility.

* Corresponding author. School of Materials Science and Engineering, Tianjin University, Tianjin, 300072, PR China.
E-mail address: xhxutju@gmail.com (X. Xu).

https://doi.org/10.1016/j.jpowsour.2018.09.096
Received 7 June 2018; Received in revised form 18 September 2018; Accepted 28 September 2018
0378-7753/ © 2018 Elsevier B.V. All rights reserved.

1. Introduction

The rapid growing of portable and wearable electronics essentially require unremitting pursuit in high-performance, multi-purpose and easily accessible energy storage devices [1–4]. Micro-supercapacitors (MSC) with planar integrated electrode have been regarded as next-generation configuration and widely used in wearable electronics with the advantages of high power density, fast charge–discharge rate, ultra-long cycle life as well as facilitated ion transport caused by the miniaturized structure [5,6]. This miniaturized structure, however, leads to difficulties in its processing; although existing micro-fabrication technologies (e.g., inkjet printing [6], screen (or stencil or blade) printing [7], laser writing [8], spray coating [9], roll-to-roll printing [10], electrophoretic deposition [11], molding [12], brush writing [13] and pencil drawing [14]) have shown great potential and excellent creativity, the usage scenarios of MSC are still limited due to the following disadvantages. Firstly, the substrate which needs to be designed and made in advance is used for most energy storage devices, limiting the application in a variety of cases and showing poor compatibility with basic components of wearable devices, such as textile, paper, or plastic [15]. Nearly all of planar devices can only be formed on a tailored substrate instead of being printed directly on the desired non-standard surface. Secondly, some supercapacitors with innovative structures require the use of additional masks or molds, resulting in high costs and low feasibility for scalability [12,15]. Thirdly, many forming methods of MSCs relying on artificial process lead to the uneven mass of each device, which would affect the electrochemical performance of the equipments. Last but the most important, fabrication methods of the electrode and electrolyte materials are often mutually exclusive, leading to the difficulty in manufacturing those materials in the same way. Consequently, only a few studies involved all-printed energy storage systems. Lee et al. fabricated the all-printed supercapacitors by controlling the viscosity of electrode ink and ionic liquid electrolyte ink via inkjet printing [16]. However, the viscosity regulation of inks is troublesome, and not all materials are available for inkjet printing. Wang and coworkers utilized screen printing to realize the all printed Zn-Ag_2O battery in the shape of “NANO” [17], which still left limits for further applications owing to the usage of additional masks. Chen and cooperators utilized the specific wetting/dewetting behavior of eGaIn liquid metal on different surfaces to fabricate all-printed quantum dot LEDs, but few materials have this characteristic [18]. Consequently, MSCs are urgently need to be fabricated in a low-cost, multi-purpose, massive-scalable, substrate-versatile way.

Direct ink writing (DIW) is a 3D printing technique in which prepared ink is extruded from a nozzle that moving across the platform [19]. This technique has been widely used in multi-material manufacturing which including energy storage devices and other applications [20–22]. Those studies about 3D printed energy storage devices mainly focused on the graphene based stereoscopic electrodes [23–27]. Despite the good rate ability and cycle ability delivered by graphene based materials, the main bottleneck is the suboptimal energy density owing to the restrict of electric double layer capacitance [1,14,28]. Compared with graphene based materials, pseudo-capacitance produced by faradic redox reactions offers high capacitance and inferior cycle performance. Conductive polymers are widely used as typical pseudo-capacitive materials with ultrahigh theoretical capacitance, low cost, little contamination and adjustable structure, and become popular in energy storage devices [2,14,15,29–34]. Thus, composite electrode materials with synergistic effect are very suitable for MSCs. DIW requires stable, shear-thinning and homogeneous dispersed ink materials for 3D printing [19]. However, common conductive polymers (such as polypyrrole (PPy) and polyaniline (PAni)) have poor dispersibility in water and can only be stably dispersed in organic solvents. But organic solvents are usually toxic and need post-processing. More importantly, they would corrode the plastic substrate and paper, thereby impairing the versatility of the substrates. Another way is to add dispersant to the inks, but the dispersant is electrochemically inert, which would affect the final electrochemical performance of the device. Therefore, building suitable inks is the key for successful 3D printed high-performance substrate-versatile MSCs.

Herein, we reported a reliable process for scalable fabrication of all-printed solid-state MSCs based on polymer/graphene materials and its *in situ* fabricated applications. The composite electrode ink contained only electroactive substances with good stability and showed significant shear thinning behavior. Note that using water as green solvent renders this composite aqueous electrode ink environmental friendly, drying safety, low cost and substrate versatility. Polyvinyl alcohol (PVA) gel is the most commonly used solid electrolyte at present. Due to its processing difficulty caused by high viscosity, it is generally coated on the surface of the electrode. The previously reported all-printed devices used low viscosity ionic liquids as electrolytes and we printed this higher viscosity PVA gel with an inconvenient patterning for the first time. Based on the green and stable inks, we printed the MSCs on different substrates and all the devices showed similar performance, with the highest performance up to 151.2 mF/cm^2. It is noted that this ink with good processability can be printed directly on the non-customized substrates. As a conceptual exhibition, we designed two schemes of *in situ* fabricated energy storage devices to meet the ever-changing energy needs and expand the application range of micro-supercapacitors. The first one is to make a transferable device by directly printing the electrode on the tape. The obtained tape-type MSCs can be stuck to any surfaces where energy is needed immediately. This is the first time to use such a simple method to produce transferable devices. The other one is an *in situ* fabricated wearable MSC with promising performance and outstanding flexibility, which was directly printed on top of a lab-gown.

2. Experimental section

2.1. Synthesis of GO and PPCANT

Graphene oxide (GO) were prepared with the modified Hummer's method. In brief, concentrated H_2SO_4 (25 mL) was added to a 250 mL beaker and heated to 90 °C. Then, $K_2S_2O_8$ (5 g) and P_2O_5 (5 g) were added successively, followed by the slow addition of graphite powder (5 g). The mixture was heated at 90 °C for 5 h. After cooling, the mixture was diluted with deionized water and stayed overnight. The mixture was then vacuum-filtered and washed with deionized water and stored at pH ≈ 7. Finally, the solid product was dried in air at room temperature. To obtain PPy nanotubes, 0.675 g $FeCl_3{\cdot}6H_2O$ was dissolved in 50 mL 5 mM methyl orange (Sigma-Aldrich) solution and 175 μL pyrrole monomer (Sigma-Aldrich) was added to the above solution with stirring for 24 h. Using deionized water and ethanol to filter precipitate until filtrate was colorless and freeze-dryed for 12 h into PPy membrane. The membranous PPy was then sliced into several square pieces (about 1.0 cm^2) as the backbones for the growth of PAni shell. The electrodeposition of aniline (Energy Chemical) was carried out in a three-electrode cell using a Pt counter electrode, an Ag/AgCl reference electrode and prepared PPy membrane as the working electrode. The electrolyte was composed of 0.5 mL aniline and 100 mL of 0.01 M H_2SO_4. Electrochemical polymerization was performed through galvanostatic electrolysis at a current density of 1.0 mA cm^{-2} for 0.5 h. After cleaning with deionized water for three times, the PPy/PAni coaxis nanotube (PPCANT) membrane was obtained.

2.2. Preparation of electrode and electrolyte inks

The PPCANR membrane was pulverized using a mortar and pestle to produce a powder. To obtain the electrode ink, 120 mg PPCANT powder, 60 mg GO powder, 20 mg conductive carbon black were dispersed in 10 mL deionized water and sonicated for 6 h. The gel electrolyte ink was prepared by mixing 1 g PVA powder (average degree of

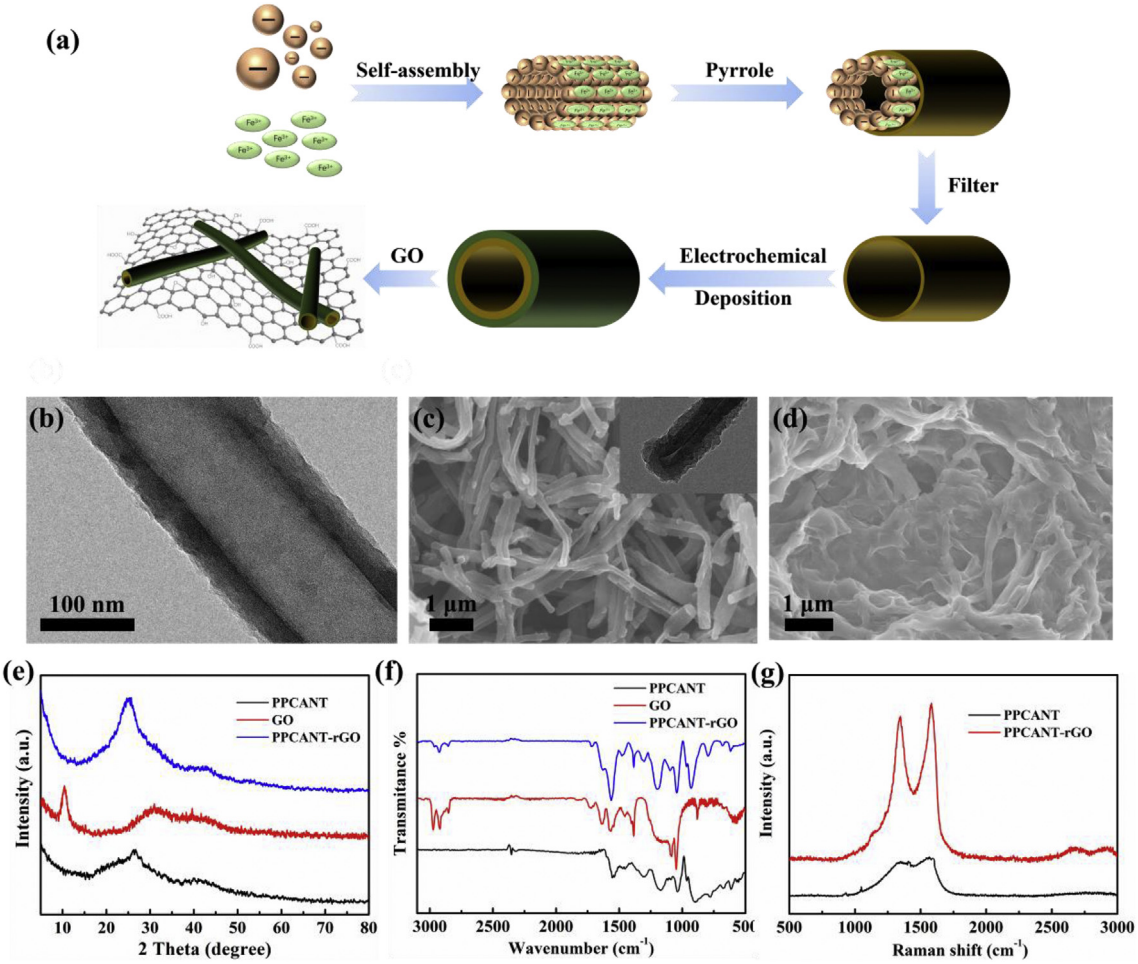

Fig. 1. Synthesis route and characterization of electrode materials. (a) Schematic illustration of the formation of the electrode ink. (b) Transmission electron microscope (TEM) image of PPy nanotubes (c) Scanning electron microscope (SEM) image of PPCANT, the inset is TEM image of PPCANT. (d) SEM image of the surface of chemically reduced electrode. (e) XRD patterns and (f) FT-IR spectra of PPCANT, GO, and PPCANT-rGO materials, respectively. (g) Raman spectra of PPCANT and PPCANT-rGO.

polymerization is 1750 ± 50, degree of alcoholysis is 87.0–89.0, Meryer), 1 mL phosphoric acid (85%, Sigma-Aldrich) and 9 mL deionized water together and heated to 85 °C until the solution became clear.

2.3. 3D printing process

The electrode ink was put in a 1 mL syringe attached to a plastic head with an inner diameter of 410 μm. The difference in electrolyte ink was the use of plastic dispensing head with an inner diameter of 840 μm. A multi axis micropositioning system (Prusa i3 and Ramps 1.4) was utilized for printing and the typical printing speed is 5 mm/s. The part of the nozzle is extruded by G-code-controlling screws, (the size diagram is shown in Fig. S1). The electrode ink was printed on different substrates to fabricate MSCs and other planar supercapacitors, while the layer height of electrode is 0.3 mm. Printed electrodes were chemically reduced using hydrazine hydrate and followed by printing a 0.5 mm layer of electrolyte ink on the top of the electrode. The size details of the printed MSCs are shown in Fig. S16. Finally, excess water was evaporated at room temperature in fume hood. Specially, when printing on the lab-gown, the value of the parameter flow is 120%.

2.4. Characterization

Material Characterization: The structural properties and morphology of electrode materials was acquired by a field emission scanning electron microscope (Hitachi S-4800) and high-resolution transmission electron microscope (JEM-2100F). The crystal structure of electrode materials was recorded by an X-ray powder diffraction (using Cu Kα radiation with k = 1.5418 Å). The FT-IR data was characterized by a NEXUS 870 spectrophotometer. Raman spectroscopy was performed using Raman spectrometer (DXR Microscope) with laser wavelength of 532 nm in the range of 2500–500 cm^{-1}. The TGA of samples was carried out using a synchronous thermal analyzer (NETZSCH STA449f3) via argon porosimetry and heating rate was 10 °C min^{-1}.

Electrochemical Measurements: Cyclic voltammetry (CV), galvanostatic charge–discharge measurements (GCD), and electrochemical impedance spectroscopy (EIS) measurements were used to accurately assess the electrochemical performances of the electrode materials and the assembled devices using an electrochemical working station (CHI660E, Shanghai, China). The capacitance (C_{device}) of devices was derived from GCD curves according to the following equations:

$$C_{device,GCD} = I\Delta t/\Delta V$$

where I(A) is the current, ΔV(V) is the potential drop during discharge and Δt(s) is the discharge time.

Alternatively, areal capacitance (C_{device}) of devices can be derived from the CV curves using the equation:

$$C_{device,CV} = \int Idt/(2v\Delta V)$$

where v is the scan rate.

The specific capacitance (C_s) of devices was calculated according to the equations:

$$C_{areal} = C_{device,GCD}/A$$
$$C_{volumetric} = C_{areal}/h$$
$$C_{mass} = C_{device,GCD}/m$$

where A is the area of electrode, m represents the total mass of both electrodes.

The energy density (E) and average power density (P) were calculated as follows:

$$E = C_s \Delta V^2/2$$
$$P = E/\Delta t$$

Δt is the discharge time (h).

The real (C') and imaginery (C'') capacitance (CA) of the devices was calculated from EIS spectra by the equation:

$$C' = \frac{-Z''}{2\pi f|Z|^2} \quad C'' = \frac{Z'}{2\pi f|Z|^2}$$

where f is frequency (Hz), Z'' is the imaginary resistance (Ω), Z' is the real resistance (Ω) and $Z = \sqrt{Z'^2 + Z''^2}$ is the overall complex impedance.

3. Results and discussion

The preparation process of the electrode ink is schematically illustrated in Fig. 1a. PPy nanotubes were fabricated through a reactive self-degraded template polymerization method. In brief, methyl orange with hydrophilic edge group (SO_3^-) is anionic characteristic in aqueous solution. $FeCl_3$ was considered to act as flocculant and could achieve complexation with methyl orange to construct fibrillar seed templates. The polymerization process of pyrrole took place on the surface of templates with assistance of Fe^{3+}. Meanwhile, the templates degraded automatically due to the reduction of oxidizing cations and gave rise to the formation of hollow nanotubular PPy. The obtained PPy nanotubes were identified to have diameters of ~160 nm and length of ~5 μm in Fig. 1b. The hollow nanotube structure can provide shear-thinning behavior for 3D printing and alleviate the volume expansion during the cycle. PPCANT was formed by *in situ* electrochemical polymerization of aniline, which is shown in Fig. 1c. It is found that the wall thickness of polyaniline is about 20 nm by comparing the parts of different contrast. The electrode ink was obtained by mixing PPCANT, GO and conductive carbon black with a certain proportion. After the electrode printing completed, hydrazine hydrate was used to reduce GO (rGO). Fig. 1d shows the morphology of the printed electrode. PPCANT were wrapped and interacted with wrinkled GO through π-π stacking interaction, so that ions could be transported rapidly between electrode layers. In addition, this interconnected network structure also played an important role in stabilizing PPCANT to enhance the electrode material stability during charge–discharge process.

Fig. 1e shows the X-ray diffraction (XRD) patterns of PPCANT, GO and PPCANT-rGO. The change of diffraction peak from 10.4° to 26.3° indicated the successful synthesis of rGO by the reduction of hydrazine hydrate [35]. For PPCANT-rGO, the characteristic peak located at 25.0° slightly skews from PPCANT, indicating that the interaction between these two components. The Fourier transform infrared (FT-IR) spectra of PPCANT, GO and PPCANT-rGO are shown in Fig. 1f. The characteristic peaks located at 1551 and 1380 cm-1 are assigned to symmetric and antisymmetric ring-stretching modes of quinone-like structure for PAni. The band at 1100 cm^{-1} is owing to C-N stretching vibration of PAni. The peaks at 1046 and 1314 cm^{-1} are attributed to C-H deformation vibrations and C-N stretching vibrations, respectively [36]. The peaks at 1636 and 905 cm^{-1} are almost consistent with the characteristic peaks of PPy reported in literature [37]. The peak at 1087 cm^{-1} represents the C-O stretching vibration [38]. For PPCANT-rGO, the peaks at 1720 and 1087 cm^{-1} are weakened, which demonstrates the reduction of GO. The synthesis of PAni and PPy were further characterized by Raman spectroscopy (Fig. 1g). It is worth noting that the intensity ratio (ID/IG) was 0.87 and 0.94 for PPCANT and PPCANT-rGO demonstrating the introduction of rGO sheets into conductive polymer matrices [39]. Moreover, the introduction of PAni also improves the heat resistance of PPy nanotubes. Thermogravimetric analysis (TGA) of PPy nanotubes, PPCANT, PPCANT-rGO are shown in Fig. S2. It can be observed that the thermal stability of PPCANT was obviously enhanced. These samples suffered about 10% weight loss at 80 °C, which is owing to the volatilization of water. From 250 °C to 400 °C, more mass losses occurred, which was attributed to the thermal decomposition of PPy. At the temperature higher than 450 °C, the skeleton of PPy began to decompose and ring opening occurs simultaneously [40]. For PPy, when the temperature reaches 800 °C, there is nearly 88% mass loss, while the coaxial nanotube composite material lost about 46% at 800 °C. It indicates that polyaniline coating plays an important role in improving thermal stability of PPy nanotubes. This may be caused by the chemical interaction between PAni and PPy, which enhances the thermal stability of the composite electrode materials. Furthermore, the addition of PAni components greatly improves the conductivity of PPy nanotubes (electrical conductivity measured by four-probe method increased from 622 S m^{-1} to 2893 S m^{-1}), which is mainly attributed to the enhancement of the π-π conjugation. The acid electrolyte environment during electrode reaction is beneficial to the doping and dedoping processes of the conductive polymers, which would further promote the electrical conductivity. Due to the excellent conductivity of graphene, PPCANT-rGO also shows a good electrical conductivity of up to ~6000 S m^{-1}, allowing the planar electrodes as well as metal-free current collectors and interconnects to be printed in single step [41,42].

Ink properties, especially the rheological behavior and stability, significantly influence the printing process and its performance. Pure GO ink exhibits shear-thinning behavior, which reveals that it is non-Newtonian fluids and can be 3D printed [43]. As shown in Fig. 2a, the composite electrode ink exhibits similar shear-thinning behavior with pure GO inks. The shear-thinning characteristics are mainly derived from the orientable nanostructures of electrode materials. For GO, due to its platelet nanostructure, the orientation will occur along the radial direction under shear stress [23,25,43]. For tubular PPCANT, the orientation is along the axial direction in order to reduce the flow resistance which would lead to a decline in viscosity and modulus. In contrast to pure GO ink, one obvious difference of the composite electrode ink is the lower viscosity of electrode ink compared in same concentration (Fig. S3), which indicate that the interaction between PPCANT and GO is weaker than the interaction of pure GO sheets. This shows that at the same viscosity, our composite electrode ink can provide more active material loading than pure GO ink. Fig. 2b displays the storage modulus and loss modulus of the composite electrode ink. At the plateau range from 10^0 to 10^2 Pa, the storage modulus is much higher than the loss modulus demonstrating a solid-like state ink. With the increase of shear stress, the loss modulus becomes higher than the storage modulus, which demonstrates that viscous deformation starts to dominate the viscoelastic ink properties. In this region, inks exhibit good fluidity, ensuring stable flowing during continuous extrusion. Thus, these plateau modulus values and viscous deformation are essential to the shaping and preserving of vertical structures for 3D printed integrated electrode.

Generally, the stability of ink can be improved by changing the base liquid or adding dispersant. But the great amount of organic solvents is corrosive to the substrates and the after treatment is tedious, which would blemish the versatile substrate. On the other hand, most dispersants are electrochemical inert, which would affect the electrochemical performance of the energy storage devices. As is known, water is the most commonly used solvent with low price and little contamination. But pure PPCANT aqueous ink is extremely easy to

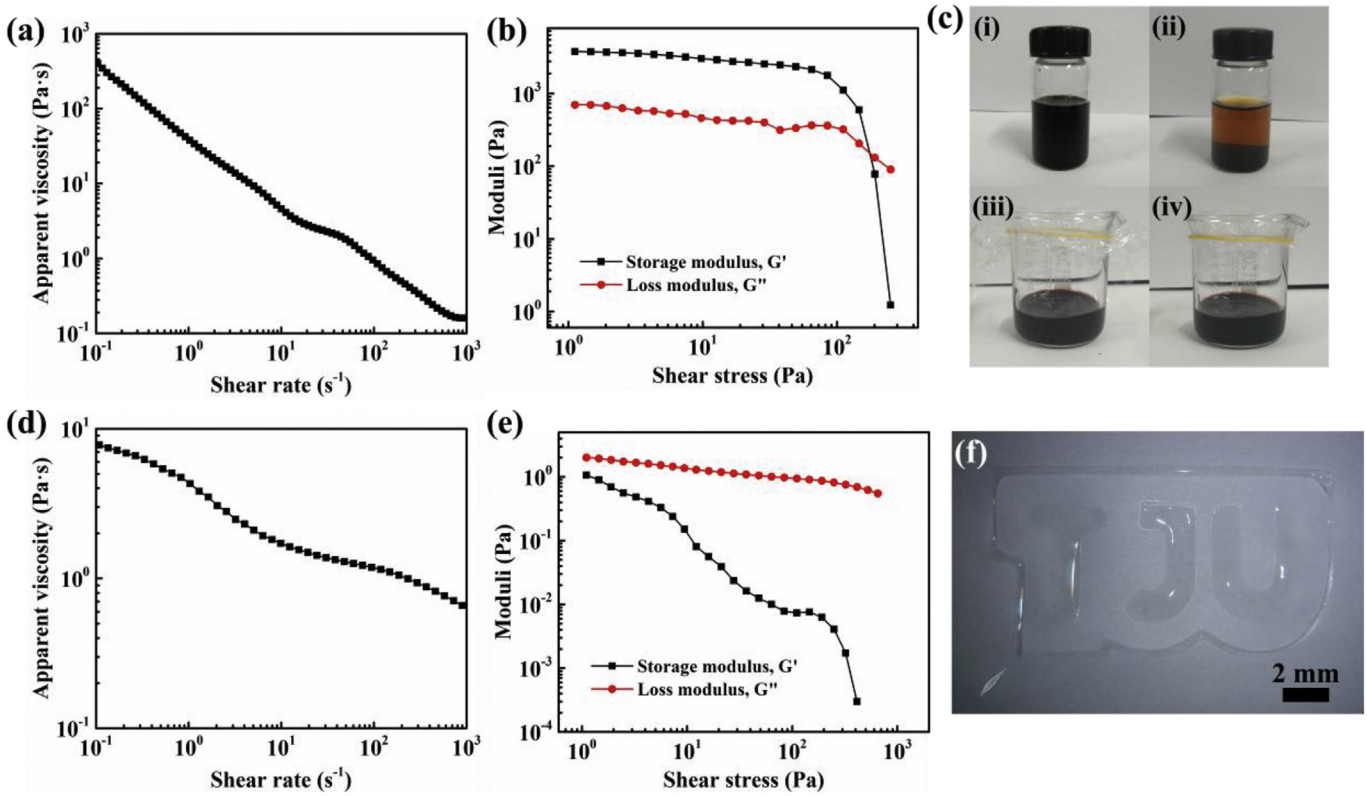

Fig. 2. Rheological properties of the composite electrode ink and electrolyte ink. (a) Apparent viscosity as a function of shear rate for composite electrode ink. (b) Storage modulus, G′, and loss modulus, G″, as a function of shear stress for the composite electrode ink. (c) The contrast diagrams between pure PPCANT aqueous ink (fresh ink (i) and standing for 4h (ii)) and composite electrode ink (fresh ink (iii) and standing for 12h (iv)). (d) Apparent viscosity as a function of shear rate, and (e) Storage modulus, G′, and loss modulus, G″, as a function of shear stress for the electrolyte ink. (f) Photograph of the electrolyte patterning in the shape of "TJU".

coagulate, which would block the nozzle and generates unstable flow during the printing process. We found that the addition of GO significantly improves the time stability, and the contrast diagram can be seen in Figs. 2c and S4. In fact, GO also plays the role of stabilizer in the composite electrode ink. Compared with the fresh ink, the apparent viscosity of electrode ink only slightly increased during the 4 weeks as shown in Fig. S5. This little change can be explained as the agglomeration of electrode materials.

PVA gel, one of the most commonly used solid electrolyte at present, was generally coated on the surface of the electrode instead of printing method due to its processing difficulty caused by high viscosity. Fig. 2d shows its viscosity is much higher than the allowable range of inkjet printing (most inkjet printing requires low viscosity less than 0.02 Pa s [6,16]). As shown in Fig. 2e, when the shear stress rises at the beginning of extrusion, the storage modulus decreases rapidly, mainly due to the destruction of the gel network structure in PVA gel. When the extrusion process ends, there is no shear stress. Because of the hydrogen bond, physical crosslinking has reoccurred, resulting in a rise in viscosity and modulus. The shear-thinning behavior makes it possible to directly print the gel into designed patterns, which providing another method for all-printed energy storage devices (A printed example with inconvenient structure can be seen in Fig. 2f). In addition, factors including the kind of acid, experimental temperature, alcoholysis degree and polymerization degree of PVA could affect the intramolecular hydrogen bond of electrolyte ink, which further influence the rheological behavior and printing quality.

Fig. 3 illustrates the fully printing process of MSC via DIW. First, electrode ink was extruded in designed sequence of MSC on the required substrate. Subsequently, the part of integrated electrode was printed on the top of the previous layer as shown in the inset and video. After the printed electrode ink is dried, GO was reduced by reducing agent (hydrogen iodate or hydrazine hydrate). Then the electrolyte ink was printed upon the electrode and displayed a slightly larger area than the area of integrated electrode. Finally, after evaporating the excess water, the all-printed solid-state MSC with multi-layer was built.

Paper is an ideal soft substrate for portable and wearable electronics due to its wide availability, low cost, light weight, environmental friendliness, bendability, flexibility and recyclability [14,16,32]. Especially for supercapacitors, the rough structure of paper can enhance the adhesion between electrode materials and substrate and ion transportation [32]. Compared with traditional cellulose paper, limestone paper mainly composed of calcium carbonate, which has better mechanical properties and does not need to cut trees. With effort to exploit these features, we mainly studied the electrochemical properties of all-printed solid-state MSCs on limestone paper. In addition, this fabrication process can be easily scaled up without redundant pre-designed masks as shown in Fig. S6. When the ink was printed at the beginning, there is sometimes a problem of uneven extrusion. In order to improve the qualified rate of large-scale printing, we printed a "Skirt" in advance on the outer edge of the device.

The areal and volumetric capacitance of the supercapacitors with different layers is shown in Fig. 4a and Fig. S7, respectively. The typical thickness of one layer is about 1.3 μm as seen in Fig. S8. Obviously, with the increase of electrode layers, the areal capacitance is greatly improved. Among them, the 4-layer MSC shows an ultrahigh areal capacitance of 151.2 mF/cm^2 at a scan rate of 5 mV s^{-1}, which mainly attribute to the maximum mass loading. Unfortunately, like other types of supercapacitors, the higher areal capacitance and gravimetric capacitance cannot be achieved simultaneously. As show in Fig. S9, gravimetric capacitance decreases as the mass loading of electrode materials increases. (The mass loading is calculated by the G-code of printing process.) Although 3D printing technology makes the fabrication of supercapacitors more facile, uniform and diversified, there still exists one problem that it doesn't make full use of the complete capacitance of

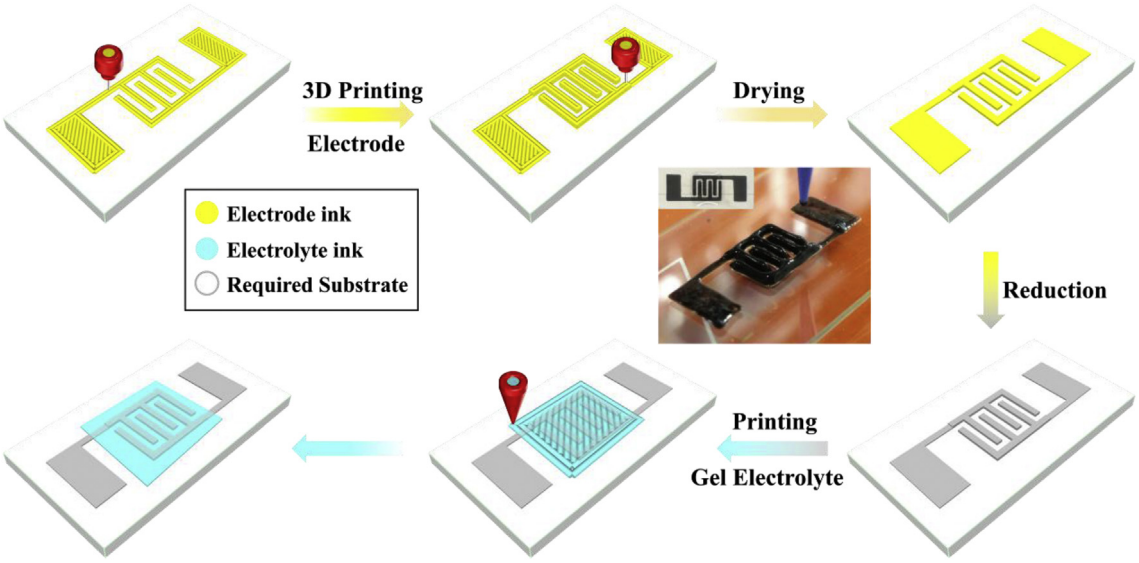

Fig. 3. Schematic illustration of the fabrication process of all-printed MSC with different layers.

materials. This leads to the lower specific capacitance of the material and restricts the practical application of the novel electrode materials. It is noteworthy that the gravimetric capacitance of our flexible solid-state supercapacitors is outstanding in the supercapacitors formed by 3D printing technology, mainly due to the addition of pseudo-capacitive materials and no electrochemical inert materials in electrode and electrolyte inks (Fig. S10).

The MSC with different layers all showed near-rectangular CV curves with wide peaks in shape at scan rate of 10 mV s^{-1} (Fig. 4b), which indicates the interaction of double layer behavior and pseudo-potential behavior [44]. It is suggested the highly efficient electrochemical reaction of the MSC with different layers. The detail CV curves with the potential window of 0–1.0 V from 5 mV s^{-1} to 100 mV s^{-1} are shown in Fig. S11 (a)-(c). Galvanostatic charge–discharge (GCD) curves of the devices with different layers at current density of 0.48 mA cm^{-2} is shown in Fig. 4c. The nearly symmetric charge and discharge curves

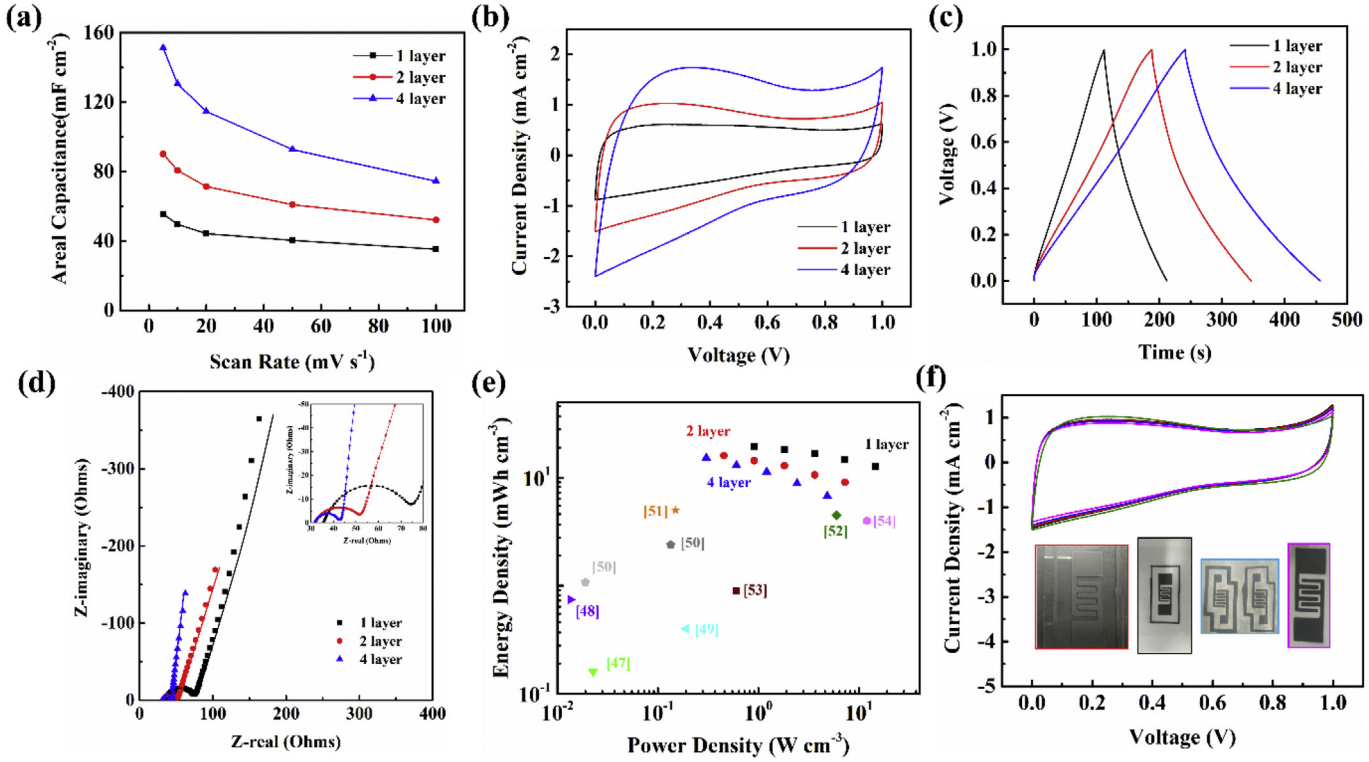

Fig. 4. Electrochemical performance of the all-printed MSC with different layers. (a) Areal capacitance as a function of scan rate for the devices with different layers. (b) CV curves for the multi-layer devices at scan rate of 10 mV s^{-1} (c) GCD curves for the devices with different layers at current of 0.48 mA cm^{-2}. (d) Nyquist plots and fitting results of the device with different layers. Inset exhibits the magnified plots in the high-frequency region. (e) Ragone plot of the all-printed multi-layer MSC and recent literature reports [47–54]. (f) CV curves of 2-layer MSCs on different substrates at scan rate of 10 mV s^{-1} (red: slide glass; black: polyethylene film; blue: weigh paper; pink: glazed printing paper; Green: limestone paper). (For interpretation of the references to color in this figure legend, the reader is referred to the Web version of this article.)

confirm the desirable capacitive behavior of these devices, which is consistent with the CV results. The coulombic efficiency of the 1-layer, 2-layer and 4-layer devices at current density of 0.48 mA cm^{-2} is 90.5%, 87.1% and 88.2%, respectively. The total GCD curves with different current densities are shown in Fig. S12 (a)-(c). Cycling performance of the 4-layer MSC is shown in Fig. S13 by using repeated GCD. It is obvious that in the initial 500 charge–discharge cycles, the specific capacity was almost constant. Then when the number of cycles raised, the specific capacitance slightly decreased. Conductive polymer electrodes often suffer the cycle degradation issues caused by mechanical problems, that is, the swelling and shrinking during the charge–discharge (doping-dedoping) process [34]. Such good electrochemical stability achieved here for conductive polymers can be attributed to the well-formed PPCANT-rGO networks as shown in Fig. 1d. Fig. 4d presents the Nyquist plot of the devices with different layers. All the plots show an inclined line in the low-frequency region and a semicircle in the high-frequency region, which correspond to the ion diffusion process within the integrated electrode and the charge-transfer impedance between the electrode/electrolyte interface [45]. In the high-frequency region, the equivalent series resistances (ESR) of the devices with 1-layer, 2-layer and 4-layer were about 40, 22 and 13 Ω, respectively. It can be found that with the increase of the number of layers, the ESR is greatly reduced. Therefore, we assume that 3D printed multi-layer structure can be equivalent to multiple parallel integrated electrode, thus improving the overall electronic transmission efficiency. Impedance phase angles of the MSCs with different layers at different frequencies are plotted in Fig. S14. The phase angle of all the devices are close to 70° at low frequency. The real and imaginary capacitance of the devices with different layers are shown in Fig. S15. At the lowest frequency, the volumetric real capacitances of 1-layer, 2-layer and 4-layer MSCs are about 44, 37, 33 F cm^{-3}. This result is basically the same as the capacitance calculated by CV method at low scan rate. Another point worth noting is that the imaginary capacitance is increasing as the number of layer increases. This maybe lead to the energy dissipation of the devices [29,46]. The equivalent circuit of the MSCs with different layers is shown in Fig. S16, according to the measured AC impedance dates. We found that different layers of devices can be represented by the same identical model.

The performance of our all-printed flexible solid-state MSCs is compared with other flexible solid-state devices reported in the literature in Ragone plot as shown in Fig. 4e. The highest energy density of all-printed flexible solid-state MSC was calculated to be 19.6 mW h cm^{-3} at power density of 0.91 mW cm^{-3}, which showed promising electrochemical performance. In addition, the MSCs also can be fabricated on other substrates. As shown in Fig. 4f, the devices with 2 layers were printed on slide glass (black), polyethylene film (red), glazed printing paper (blue) and weigh paper (pink) (the integrated electrode part is same as that on limestone paper). Obviously, the change of substrates does not affect the performance of the MSCs much: more than 88% capacitance can be retained on different substrates. Accordingly, all the data reveals a stable and high-performance MSCs, which is applicable in various situations.

To meet the specific energy and power needs for practical applications, we printed an integrated MSC in series configurations (Fig. 5a). The integrated MSC showed almost unchanged charge–discharge time compared with the single device at the same current density with an increased voltage window by 3 times. Most of the planar MSCs are made up of simple straight lines. In order to demonstrate the good formability of this electrode inks, we have designed a complex badge-like planar supercapacitor with curvilinear lines and the print preview is shown in Fig. 5b (the area of the two electrodes is equal). Compared with the previous patterns, the printing of Fig. 5b takes as many as 484 retractions (In order to improve the print quality, it is often necessary to retract the inks when the nozzle is not extruding). Fig. 5c exhibits the final printed result by using the composite electrode ink. It can be seen that the two have almost the same shapes and details, showing exceptionally aesthetics and potential applicability as a state-of-the-art class of object-tailored energy storage. For all we have known, this is the most complicated planar supercapacitors made by 3D printing technology and the device also shows expected capacitance (Fig. S17).

Previous studies have shown that energy storage devices can be formed on different substrates in many novel ways. However, almost all of them was fabricated on the prepared substrate and then assembled in a certain way. Therefore, it is a challenge to bring electronic equipment closer to the required application scene and reduce intermediate procedures. As a conceptual attempt, we have designed two *in situ* fabricated energy storage applications to meet the ever-changing demand of energy sources and expand the molding range of energy storage equipment.

The mentioned above and some literature demonstrated that the MSCs can be printed on different substrates and all the substrates used are fixed, preventing the electronic devices transferring quickly and easily to another surface. However, when it is urgently needed for energy on indeterminate surface, it is always impossible to print on site and on time and also very expensive to fix batteries on all substrates at the same time. Furthermore, we sometimes hope that batteries can be placed on any surface rather than blocked in one kind of shell, or fixed on only one surface. Therefore, a device that can be quickly and easily transferred has its unique application value. As shown in Fig. 5d, the MSCs can be printed on the planar polyethylene tape in the same way as mentioned above. Then remove the printed tape-type device and paste it to the desired surface under special requirements. For example, the MSCs were transferred onto the flat or curved surface (beaker, wood, cloth, and wall) as shown in Fig. 5e, which exhibits the excellent substrate versatility of the as-developed facile transfer process.

Electrode materials can be made into wearable energy storage devices in numerous ways at present, however, almost all methods reported require subsequent processing of the as-obtained devices. For example, weaving fibers into textile and sewing the cloth to fabric. Few literature has ever reported that electrode materials can be directly molded into everyday clothes and we propose a simpler way to make wearable supercapacitors. Besides being printed to the pre-cut substrates as used above, the MSCs can also be printed directly on the required cloth surface. As shown in Fig. 5f, the device was directly printed to a common lab-gown via the same 3D printer as the previous. Because the clothing fibers would absorb solvents, the printing parameters were different from before. Because the clothing fibers, made of cotton, would absorb solvents, the printing parameters were different from before (the value of the parameter flow is 120%). In addition, the *in situ* fabricated MSCs exhibit promising electrochemical performance via CV and GCD experiments as shown in Figs. S18 and S19. The *in situ* fabricated MSCs also exhibited excellent capacitance stability under different bending radius (Fig. S20). The CV curves all showed nearly identical trend at 50 mV s^{-1}, indicating the negligible variation of the capacitive behavior. When bending radius turned to 1.0 cm, the capacitance retention rate can still reach 94%, indicating that the device can maintain good toughness and energy storage property under bending. This provides the basic conditions for the application of the *in situ* fabricated MSCs in flexible wearable electronic devices. As a prospect, this method may open a facile door of *in situ* printed micro energy storage devices for portable and wearable electronics application.

4. Conclusion

In summary, we demonstrated a novel all-printed method to fabricate solid-state planar MSCs on different substrates via 3D printing. The aqueous electrode ink used exhibited significant shear-thinning rheological properties, remarkable time stability and outstanding electrochemical performance. The printing of PVA gel displayed a new method to form solid-state electrolyte with inconvenient structure. The all-printed multi-layer MSCs showed excellent electrochemical performance: the areal capacitance of 4-layer device is up to 151.2 mF/cm^2

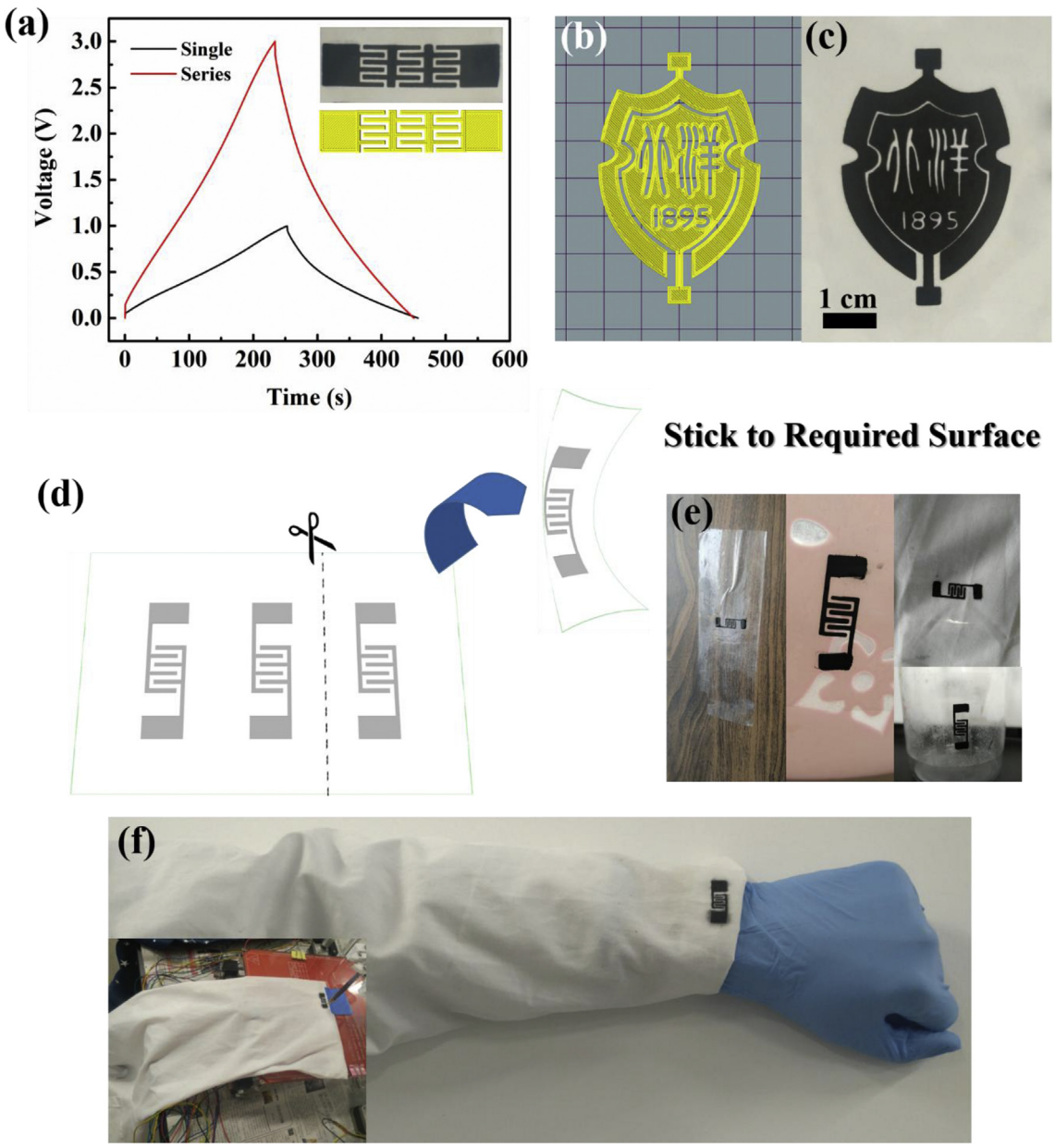

Fig. 5. Further application of the planar MSCs. (a) GCD curves of the 4-layer MSC as-discussed and the integrated 4-layer MSC in series at fixed 0.2 mA. Inset: Digital photograph and printed preview of the integrated MSC in series. (b) Print preview of the planar electrodes in the shape of badge. (c) Digital photograph of the printed device in the shape of badge. (d) Schematic diagram of the tape-type MSCs. (e) Photographs of the tape-type MSCs on different substrates (wood, plastic, texile and glass). (f) Image of the printed device on lab-gown.

and the highest volumetric energy density is 19.6 mW h cm^{-3} at average power density of 0.91 mW cm^{-3}. In addition, inks had good compatibility with a variety of substrates (paper, glass, texile, etc), and even allowed *in situ* fabricated on the required surface. Based on these, the *in situ* fabricated tape-type MSCs can be easily and quickly transferred to various surfaces, enabling one electronic device to be transferred to different locations. The *in situ* fabricated MSC on lab-gown showed promising performance and excellent flexibility, which may provide a new idea for wearable micro energy storage equipment.

Acknowledgements

This project was financially supported by the National Natural Science Foundation of China (no.51143009 and 51273145). The authors gratefully acknowledge Dr. Xiaohui Li and Mr. Xilin Huang for their helpful discussion.

Appendix A. Supplementary data

Supplementary data to this article can be found online at https://doi.org/10.1016/j.jpowsour.2018.09.096.

References

[1] Y. Wang, Y. Song, Y. Xia, Electrochemical capacitors: mechanism, materials, systems, characterization and applications, Chem. Soc. Rev. 45 (2016) 5925.
[2] L. Wang, D. Chen, K. Jiang, G. Shen, New insights and perspectives into biological materials for flexible electronics, Chem. Soc. Rev. 46 (2017) 6764.
[3] J. Zhao, H. Li, C. Li, Q. Zhang, J. Sun, X. Wang, J. Guo, L. Xie, J. Xie, B. He, Z. Zhou, C. Lu, W. Lu, G. Zhu, Y. Yao, MOF for template-directed growth of well-oriented nanowire hybrid arrays on carbon nanotube fibers for wearable electronics integrated with triboelectric nanogenerators, Nanomater. Energy 45 (2018) 420.
[4] Y. Gogotsi, P. Simon, True performance metrics in electrochemical energy storage, Science 334 (2014) 917.
[5] N.A. Kyerematen, T. Brousse, D. Pech, Microsupercapacitors as miniaturized

energy-storage components for on-chip electronics, Nat. Nanotechnol. 12 (2016) 7.
[6] Y. Wang, Y. Zhang, D. Dubbink, J.E. Ten Elshof, Inkjet printing of δ-MnO2 nanosheets for flexible solid-state micro-supercapacitor, Nanomater. Energy 49 (2018) 481.
[7] Y. Xu, M.G. Schwab, A.J. Strudwick, I. Hennig, X. Feng, Z. Wu, K. Müllen, Screen-printable thin film supercapacitor device utilizing graphene/polyaniline inks, Adv. Energy Mater. 3 (2013) 1035–1040.
[8] J. Cai, C. Lv, A. Watanabe, Laser direct writing of high-performance flexible all-solid-state carbon micro-supercapacitors for an on-chip self-powered photodetection system, Nanomater. Energy 30 (2016) 790.
[9] S. Tuukkanen, M. Välimäki, S. Lehtimäki, T. Vuorinen, D. Lupo, Behaviour of one-step spray-coated carbon nanotube supercapacitor in ambient light harvester circuit with printed organic solar cell and electrochromic display, Sci. Rep. 6 (2016) 22967.
[10] J. Yeo, G. Kim, S. Hong, S.K. Min, D. Kim, J. Lee, H.B. Lee, J. Kwon, Y.D. Suh, H.W. Kang, Flexible supercapacitor fabrication by room temperature rapid laser processing of roll-to-roll printed metal nanoparticle ink for wearable electronics application, J. Power Sources 246 (2014) 562.
[11] S. Xu, G. Wei, J. Li, Y. Ji, N. Klyui, V. Izotov, W. Han, Binder-free $Ti_3C_2T_x$ MXene electrode film for supercapacitor produced by electrophoretic deposition method, Chem. Eng. J. 317 (2017) 1026.
[12] W.J. Hyun, E.B. Secor, C.H. Kim, M.C. Hersam, L.F. Francis, C.D. Frisbie, Scalable, self-aligned printing of flexible graphene micro-supercapacitors, Adv. Energy Mater. 7 (2017) 1700285.
[13] J. Li, Y. Shao, Q. Shi, C. Hou, Q. Zhang, Y. Li, R.B. Kaner, H. Wang, Calligraphy-inspired brush written foldable supercapacitors, Nanomater. Energy 38 (2017) 428.
[14] B. Yao, L. Yuan, X. Xiao, J. Zhang, Y. Qi, J. Zhou, J. Zhou, B. Hu, W. Chen, Paper-based solid-state supercapacitors with pencil-drawing graphite/polyaniline networks hybrid electrodes, Nanomater. Energy 2 (2013) 1071.
[15] M. Zhu, Y. Huang, Y. Huang, H. Li, Z. Wang, Z. Pei, Q. Xue, H. Geng, C. Zhi, A highly durable, transferable, and substrate-versatile high-performance all-polymer micro-supercapacitor with plug-and-play function, Adv. Mater. (Weinheim, Ger.) 29 (2017) 1605137.
[16] K.H. Choi, J.T. Yoo, K.L. Chang, S.Y. Lee, All-inkjet-printed, solid-state flexible supercapacitors on paper, Energy Environ. Sci. 9 (2016) 9.
[17] R. Kumar, J. Shin, L. Yin, J.M. You, Y.S. Meng, J. Wang, All-printed, stretchable Zn-Ag2O rechargeable battery via hyperelastic binder for self-powering wearable electronics, Adv. Energy Mater. 7 (2017) 1602096.
[18] Y. Jiang, S. Su, H. Peng, H. Sing Kwok, X. Zhou, S. Chen, Selective wetting/de-wetting for controllable patterning of liquid metal electrodes for all-printed device application, J. Mater. Chem. C. 5 (2017) 12378.
[19] J.A. Lewis, Direct ink writing of 3D functional materials, Adv. Funct. Mater. 16 (2010) 2193.
[20] F. Zhang, M. Wei, V.V. Viswanathan, B. Swart, Y. Shao, G. Wu, C. Zhou, 3D printing technologies for electrochemical energy storage, Nanomater. Energy 40 (2017) 418.
[21] X. Tian, J. Jin, S. Yuan, C.K. Chua, B.T. Shu, K. Zhou, Emerging 3d-printed electrochemical energy storage devices: a critical review, Adv. Energy Mater. 7 (2017) 1700127.
[22] M. Wei, F. Zhang, W. Wang, P. Alexandridis, C. Zhou, G. Wu, 3D direct writing fabrication of electrodes for electrochemical storage devices, J. Power Sources 354 (2017) 134.
[23] Y. Jiang, Z. Xu, T. Huang, Y. Liu, F. Guo, J. Xi, W. Gao, C. Gao, Direct 3D printing of ultralight graphene oxide aerogel microlattices, Adv. Funct. Mater. 28 (2018) 1707024.
[24] G. Sun, J. An, C.K. Chua, H. Pang, J. Zhang, P. Chen, Layer-by-layer printing of laminated graphene-based interdigitated microelectrodes for flexible planar micro-supercapacitors, Electrochem. Commun. 51 (2015) 33.
[25] W. Li, Y. Li, M. Su, B. An, J. Liu, D. Su, L. Li, F. Li, Y. Song, Printing assembly and structural regulation of graphene towards three-dimensional flexible micro-supercapacitors, J. Mater. Chem. 5 (2017) 16281.
[26] C.W. Foster, M.P. Down, Y. Zhang, X. Ji, S.J. Rowleyneale, G.C. Smith, P.J. Kelly, C.E. Banks, 3D printed graphene based energy storage devices, Sci. Rep. 7 (2017) 42233.
[27] V.G. Rocha, E. Garcíatuñón, C. Botas, F. Markoulidis, E. Feilden, E. D Elia, N. Ni, M. Shaffer, E. Saiz, Multimaterial 3D printing of graphene-based electrodes for electrochemical energy storage using thermoresponsive inks, ACS Appl. Mater. Interfaces 9 (2017) 42.
[28] A. Laheäär, P. Przygocki, Q. Abbas, F. Béguin, Appropriate methods for evaluating the efficiency and capacitive behavior of different types of supercapacitors, Electrochem. Commun. 60 (2015) 21.
[29] G.A. Ragoisha, Y.M. Aniskevich, False Capacitance of Supercapacitors, (2016) http://arxiv.org/abs/1604.08154.
[30] P. Simon, Y. Gogotsi, Materials for electrochemical capacitors, Nat. Mater. 7 (2008) 845.
[31] T. Brousse, D. Belanger, J.W. Long, To be or not to be pseudocapacitive? J. Electrochem. Soc. 162 (2015) 5185.
[32] H.P. Cong, X.C. Ren, P. Wang, S.H. Yu, Flexible graphene-polyaniline composite paper for high-performance supercapacitor, Energy Environ. Sci. 6 (2013) 1185.
[33] Y. Gao, Graphene and polymer composites for supercapacitor applications: a review, Nanoscale Res. Lett. 12 (2017) 387.
[34] Q. Meng, K. Cai, Y. Chen, L. Chen, Research progress on conducting polymer based supercapacitor electrode materials, Nanomater. Energy 36 (2017) 268.
[35] P.G. Ren, D.X. Yan, X. Ji, T. Chen, Z.M. Li, Temperature dependence of graphene oxide reduced by hydrazine hydrate, Nanotechnology 22 (2011) 55705.
[36] Z.L. Wang, X.J. He, S.H. Ye, Y.X. Tong, G.R. Li, Design of polypyrrole/polyaniline double-walled nanotube arrays for electrochemical energy storage, ACS Appl. Mater. Interfaces 6 (2014) 642.
[37] T.J. Pan, X.W. Zuo, T. Wang, J. Hu, Z.D. Chen, Y.J. Ren, Electrodeposited conductive polypyrrole/polyaniline composite film for the corrosion protection of copper bipolar plates in proton exchange membrane fuel cells, J. Power Sources 302 (2016) 180.
[38] D.C. Marcano, D.V. Kosynkin, J.M. Berlin, A. Sinitskii, Z. Sun, A. Slesarev, L.B. Alemany, W. Lu, J.M. Tour, Improved synthesis of graphene oxide, ACS Nano 4 (2010) 4806.
[39] Y. Liu, Y. Zhang, G. Ma, Z. Wang, K. Liu, H. Liu, Ethylene glycol reduced graphene oxide/polypyrrole composite for supercapacitor, Electrochim. Acta 88 (2013) 519.
[40] G. Wang, X. Fu, J. Huang, L. Wu, Q. Du, Synthesis and spectroelectrochemical properties of two new dithienylpyrroles bearing anthraquinone units and their polymer films, Electrochim. Acta 55 (2010) 6933.
[41] H. Xiao, Z. Wu, F. Zhou, S. Zheng, D. Sui, Y. Chen, X. Bao, Stretchable tandem micro-supercapacitors with high voltage output and exceptional mechanical robustness, Energy Storage Materials 13 (2018) 233.
[42] X. Shi, Z.S. Wu, J. Qin, S. Zheng, S. Wang, F. Zhou, C. Sun, X. Bao, Graphene-based linear tandem micro-supercapacitors with metal-free current collectors and high-voltage output, Adv. Mater. (Weinheim, Ger.) 29 (2017) 44.
[43] E. García-Tuñon, S. Barg, J. Franco, R. Bell, S. Eslava, E. D'Elia, R.C. Maher, F. Guitian, E. Saiz, Printing in three dimensions with graphene, Adv. Mater. (Weinheim, Ger.) 27 (2015) 1688.
[44] P. Simon, Y. Gogotsi, B. Dunn, Where do batteries end and supercapacitors begin? Science 343 (2014) 1210.
[45] W. Chen, R.B. Rakhi, L. Hu, X. Xie, Y. Cui, H.N. Alshareef, High-performance nanostructured supercapacitors on a sponge, Nano Lett. 11 (2011) 5165.
[46] S. Zhang, N. Pan, Supercapacitors performance evaluation, Adv. Energy Mater. 5 (2015) 6.
[47] H. Wu, K. Jiang, S. Gu, H. Yang, Z. Lou, D. Chen, G. Shen, Two-dimensional Ni(OH) 2 nanoplates for flexible on-chip microsupercapacitors, Nano Res 8 (2015) 3544.
[48] Z. Peng, R. Ye, J.A. Mann, D. Zakhidov, Y. Li, P.R. Smalley, J. Lin, J.M. Tour, Flexible boron-doped laser-induced graphene microsupercapacitors, ACS Nano 9 (2015) 5868.
[49] S.K. Kim, H.J. Koo, A. Lee, P.V. Braun, Selective wetting-induced micro-electrode patterning for flexible micro-supercapacitors, Adv. Mater. (Weinheim, Ger.) 26 (2014) 5108.
[50] L. Li, J. Zhang, Z. Peng, Y. Li, C. Gao, Y. Ji, R. Ye, N.D. Kim, Q. Zhong, Y. Yang, High-performance pseudocapacitive microsupercapacitors from laser-induced graphene, Adv. Mater. (Weinheim, Ger.) 28 (2016) 838.
[51] Y.-Z.Y. Zhang, T. Cheng, Y. Wang, W.W.-Y. Lai, H. Pang, W. Huang, A simple approach to boost capacitance: flexible supercapacitors based on manganese oxides@MOFs via chemically induced in situ self-transformation, Adv. Mater. (Weinheim, Ger.) 28 (2016) 5242.
[52] T. Göhlert, P. Siles, T. Päßler, R. Sommer, S. Baunack, S. Oswald, O. Schmidt, Ultra-Thin all-Solid-State Micro-Supercapacitors with Exceptional Performance and Device Flexibility, 33 (2017), p. 387.
[53] L. Yuan, B. Yao, B. Hu, K. Huo, W. Chen, J. Zhou, Polypyrrole-coated paper for flexible solid-state energy storage, Energy Environ. Sci. 6 (2013) 470.
[54] M.F. El-Kady, R.B. Kaner, Scalable fabrication of high-power graphene micro-supercapacitors for flexible and on-chip energy storage, Nat. Commun. 4 (2013) 1475.